HHS Public Access

Author manuscript

Nat Immunol. Author manuscript; available in PMC 2018 January 03.

Published in final edited form as:

Nat Immunol. 2017 September ; 18(9): 973–984. doi:10.1038/ni.3791.

Skewing of the population balance of lymphoid and myeloid cells by secreted and intracellular osteopontin

Masashi Kanayama[1], **Shengjie Xu**[1,*], **Keiko Danzaki**[1,*], **Jason R. Gibson**[2,3], **Makoto Inoue**[1], **Simon G. Gregory**[2,4], and **Mari L. Shinohara**[1,4,**]

[1]Department of Immunology, Duke University School of Medicine, Durham, NC 27710, USA

[2]Duke Molecular Physiology Institute, Duke University School of Medicine, Durham, NC 27710, USA

[3]Department of Medicine, Duke University School of Medicine, Durham, NC 27710, USA

[4]Department of Molecular Genetics and Microbiology, Duke University School of Medicine, Durham, NC 27710, USA

Abstract

The balance between myeloid and lymphoid populations must be well controlled. Here, we report that a protein, osteopontin (OPN), skews the balance between myeloid and lymphoid populations during pathogenic conditions, such as infection and autoimmunity. Importantly, two OPN isoforms exert distinct effects in shifting the balance through cell type-specific regulation of apoptosis. Intracellular OPN (iOPN) reduces population sizes of myeloid progenitors and myeloid cells, and secreted OPN (sOPN) increases population sizes of lymphoid cells. The total impact of OPN in skewing leukocyte population balance was observed as host sensitivity to early systemic Candida infection and T cell-mediated colitis. This study suggests novel detrimental roles of two OPN isoforms causing the imbalance of leukocyte populations.

Skewing a population balance between myeloid and lymphoid cells impacts immune responses. Thus, the hematopoietic process is tightly controlled. In contrast to steady-state hematopoiesis, physiological insults that require an acute supply of leukocytes temporarily

**Corresponding author. Department of Immunology, DUMC3010, Duke University Medical Center, Durham, NC 27710. Phone: 919-613-6977, mari.shinohara@duke.edu.

*These authors contributed equally to this work.

ACCESSION CODES

GSE99735. Comparing single cell sequences between WT vs. *Spp1*$^{-/-}$ multi-potent progenitor cells (MPP) cells.

DATA AVAILABILITY

The data that support the findings of this study are available from the corresponding author upon request.

AUTHOR CONTRIBUTIONS

M.K. performed the majority of experiments; S.X. performed parts of experiments for cell density-mediated OPN upregulation and validating LSL-iOPN mice; K.D. performed parts of BM chimera experiments; M.I. provided experimental help to generate and validate LSL-iOPN mouse line; S.G. and J.G. performed single-cell analysis, analyzed data, and provided editorial help; M.K. and M.L.S. conceived the project and wrote the manuscript.

COMPETING FINANCIAL INTERESTS

The authors declare no conflict of interests.

alter patterns of hematopoiesis. Such demand-adapted hematopoiesis is observed during severe infections, inflammation, and irradiation, and myelopoiesis becomes highly active to compensate the loss of myeloid cells[1, 2, 3, 4]. This response is called ‘emergency myelopoiesis’ (or ‘emergency granulopoiesis’ especially for the acute generation of neutrophils). Emergency granulopoiesis is triggered by stimulating pattern-recognition receptors (PRRs), reactive oxygen species, and cytokines, such as IL-6, GM-CSF, G-CSF, and others[1, 2, 3, 4, 5, 6, 7, 8, 9, 10]. Decreased cell density by depleting neutrophils can also promote granulopoiesis in the bone marrow (BM)[10]. Lymphocytes have distinct mechanisms from myeloid cells to regulate their population sizes, and a normal immune system keeps an optimal balance between myeloid and T cells.

OPN is a phosphoglycoprotein expressed in various tissues and cell types. OPN controls various immune responses and is involved in the pathogenesis of a wide variety of diseases[11, 12, 13, 14, 15, 16, 17]. OPN is expressed by BM stroma cells[18] and negatively regulates stem cell pool size and function of $Lin^{-}Sca\text{-}1^{+}c\text{-}kit^{+}$ (LSK) cells, including hematopoietic stem cells (HSCs)[19, 20, 21]. However, the impact of OPN on myeloid or lymphoid progenitors has not been explored.

OPN exists as two translational isoforms, secreted OPN (sOPN) and intracellular OPN (iOPN). They have distinct functions due to their localization[22]. The majority of OPN studies have focused on sOPN, which interacts with receptors such as integrins and CD44. In contrast, iOPN was later found as a product of alternative translation[23] and resides in the cytoplasm and occasionally in the nucleus. iOPN functions as an adaptor or scaffold protein in signal transduction pathways, as well as stabilizing other intracellular proteins[11, 13, 14, 24, 25]. Although sOPN in the hematopoietic stem cell niche in the BM is a negative regulator of HSC proliferation[19, 20], the role of iOPN in hematopoiesis is entirely unknown.

In this study, we report that OPN skews the balance of cell populations towards a decrease of myeloid and an increase of lymphoid populations. However, this happens only during demand-adapted myelopoiesis (elicited by such as irradiation and systemic fungal infection) and lymphoid cell expansion in lymphopenic recipients. We found that iOPN is responsible for the negative regulation of myelopoiesis. In contrast, sOPN enhances lymphoid cell expansion. Thus, two different OPN isoforms play distinct roles but, as a total, work together to decrease myeloid progenitors and increase lymphoid cells during demand-adapted myelopoiesis and lymphoid cell expansion in lymphopenic hosts.

RESULTS

Cell population balance in irradiation BM chimeric mice

In naïve mice, OPN-deficiency does not affect numbers of total splenocytes, total BM cells, lineage negative (Lin^{-}) progenitors, differentiated leukocytes in the BM[19, 26], as well as compositions of BM progenitor and differentiated leukocyte populations (Supplementary Fig. 1a–e). No impact of OPN was also identified in proportions of embryonic leukocyte and their progenitor populations in fetal livers among littermate embryos (E13–15) from *Spp1* (gene encoding OPN) heterozygous breeders (Supplementary Fig. 1f, g).

Next, we examined whether OPN affects the cell population balance in mixed BM radiation chimeras transferred with WT and *Spp1*$^{-/-}$ BM cells (Supplementary Fig. 2a, b). Serum OPN (*i.e.*, secreted OPN; sOPN) in the chimera were comparable to those in naive WT mice (Supplementary Fig. 2c). Seven weeks after BM cell transplant, *Spp1*$^{-/-}$ donor cells showed increased myeloid cell populations and decreased lymphoid cell populations in multiple organs including BM, spleen, blood, mesenteric lymph nodes (MLNs), liver, and lungs (Fig. 1a, b). *Spp1*$^{-/-}$ donor cells had larger populations in multipotent progenitors (MPPs), common myeloid progenitors (CMPs), and granulocyte-macrophage progenitors (GMPs), but slightly a smaller common lymphoid progenitor (CLPs) cell populations, compared to WT donor cells (Fig. 1c, d). To confirm the BM cell transfer results, we also used mixed LSK (Lin^{-}Sca-1^{+}c-kit^{+}) cells for transfer (Supplementary Fig. 2d, e), and again *Spp1*$^{-/-}$CMP and GMP populations were larger than those of WT (Fig. 1e). Furthermore, we ruled out differential homing of transferred *Spp1*$^{-/-}$ cells to BM, as shown by the unaltered donor cell ratio (1:1 of WT and *Spp1*$^{-/-}$) in HSC and progenitor populations (Lin^{-}c-kit^{+}), the LSK population (Lin^{-}c-kit^{+}Sca-1^{+}, including HSCs and MPPs), and the Lin^{-}c-kit^{+}Sca-1^{-} population (including megakaryocyte-erythroid progenitors, GMPs, and CMPs) on Day 6 in BM (Fig. 1f). Taken together, in irradiated recipients, cell-intrinsic OPN expression in hematopoietic progenitors is sufficient to reduce myeloid progenitor populations.

OPN limits emergency granulopoiesis

Peritoneal thioglycollate injection decreased the neutrophil population in the BM within 12 hr with recovery by 70 hrs (Supplementary Fig. 3a). At 24 hrs after injection, the CMP and GMP populations were significantly increased and proliferated in BM, while such behaviors were not observed in CLPs (Supplementary Fig. 3b, c). These observations reflect emergency granulopoiesis after thioglycollate injection.

In the setting of thioglycollate injection, *Spp1*$^{-/-}$ mice again showed increased GMPs and neutrophils, compared to WT mice, in BM 24 hrs after injection (Fig. 2a, b). Here, WT and *Spp1*$^{-/-}$ mice showed similar kinetics in the decrease of BM neutrophils and numbers of neutrophils recruited in the peritoneal cavity in the first 12 hrs (Supplementary Fig. 3d, e), suggesting that OPN may not affect the egress and migration of BM neutrophils. However, enhanced GMP cellularity in the *Spp1*$^{-/-}$ BM and apparently reduced neutrophils in the BM suggested OPN downregulates granulopoiesis, while the impact of OPN on CLPs and B cells was minimal in the BM (Fig. 2a, b). Thus, OPN selectively regulates granulopoiesis by reducing the GMP population.

Although serum OPN amounts were increased during the first 24 hrs after thioglycollate injection (Supplementary Fig. 3f), *Spp1* mRNA in GMPs was temporarily reduced (Fig. 2c). Based on the enhanced outcome of myelopoiesis in *Spp1*$^{-/-}$ mice (Fig. 1), we hypothesized that the temporary decrease of OPN expression in GMPs positively impacted enhanced myelopoiesis and set out to determine what downregulated the OPN expression in the myeloid progenitor cells during emergency granulopoiesis. Here, we first evaluated the cell density because we reasoned that massive cell egress by acute inflammation reduced the cell density in the stem cell niche (Fig. 2d). To recapitulate a high cell density condition *ex vivo*,

we plated GMPs in a round-bottom plate, in which cells are crowded at the bottom of wells. Indeed, GMPs in a round-bottom plate expressed higher levels of *Spp1* mRNA than GMPs in a flat-bottom plate (Fig. 2e). For further evaluation, we used BM-derived macrophages (BMMs) because of the paucity of GMPs. With BMMs, we confirmed that *Spp1* expression depends on cell density in a dosage-dependent manner (Supplementary Fig. 3g). *Spp1* expression was positively correlated to cell density, while gene expression of *Tnf, Il6, Il10*, and *Cxcl1* had a negative correlation to cell density (Supplementary Fig. 3h).

Hippo signaling induces OPN through Mst1/2 activation

To examine how cells sense cell density to regulate *Spp1* expression, we first tested the involvement of soluble factors by comparing BMM culture supernatants from round-bottom or flat-bottom plates. However, no difference was found in *Spp1* expression in cells cultured in the supernatants (Supplementary Fig. 3i). Then, we evaluated a signaling pathway activated by cell-cell contacts, which activates the Hippo pathway[27, 28, 29]. We found that BMMs cultured in round-bottom wells increased OPN protein accompanied with the activation of Mst1/2, a critical signaling molecule in the Hippo pathway[30] (Fig. 2f). Inhibition of Mst1/2 abolished cell density-mediated upregulation of *Spp1* expression (Fig. 2g), strongly suggesting the Hippo signaling induces OPN expression. Blockade of E-cadherin, known to trigger the Hippo pathway[29], decreased *Spp1* expression at least partially in BMMs plated in round-bottom wells (Supplementary Fig. 3j). Thioglycollate treatment and systemic Candida infection induced E-cadherin expression, and blockade of E-cadherin also prevented cell density-mediated *Spp1* upregulation in GMPs (Fig. 2h, i). Thus, high cell density increased *Spp1* expression through the Hippo pathway.

We next evaluated whether inflammatory stimuli downregulate *Spp1* expression by stimulating GMPs with TNF, G-CSF, GM-CSF, or lipopolysaccharide (LPS), which are known to promote granulopoiesis, but none of them greatly decreased *Spp1* expression in GMPs (Fig. 2j). Then, we evaluated whether cell egress from BM without inflammation downregulated *Spp1* expression. Mice treated with a CXCR4 antagonist decreased total BM cell counts and *Spp1* expression in GMPs (Supplementary Fig. 3k, l). Although factors other than cellularity in the BM may also be involved in downregulating *Spp1* mRNA, these results suggest that the decrease of *Spp1* mRNA *in vivo* requires low cell densities in the BM.

Emergency myelopoiesis during systemic Candida infection

Emergency granulopoiesis plays an important role in protecting hosts from systemic fungal infections such as *Candida albicans*[31, 32] by quickly generating neutrophils, which are critical for fungal clearance at an early stage of the infection. Candida infection enhanced proliferation of CMPs and GMPs, and increased their population sizes, while CLPs did not respond as CMPs and GMPs did (Supplementary Fig. 3c, m). Here, we hypothesized that OPN is detrimental at an early stage of systemic Candida infection because OPN restricts emergency granulopoiesis. Indeed, WT host survival was significantly worse than *Spp1*$^{-/-}$ host survival at 24 hrs after Candida infection (Fig. 2k) with increased fungal loads in the kidney and spleen (Fig. 2l and Supplementary Fig. 3n) in addition to a sign of elevated tissue damage (Fig. 2m). Infected WT mice showed less abundant neutrophils and Ly6C^{+}

monocytes/macrophages compared to *Spp1*$^{-/-}$ mice, while lymphoid cell populations were not altered between WT and *Spp1*$^{-/-}$ mice (Fig. 2n). WT mice also showed decreased sizes of the GMP population compared to *Spp1*$^{-/-}$ mice without affecting MPP, CMP, and CLP population sizes (Fig. 2o, p). Here, no difference was found between WT and *Spp1*$^{-/-}$ mice in major anti-fungal responses, including serum TNF, neutrophil chemoattractants (CXCL1 and CXCL2), cytokine and chemokine expression in renal neutrophils and macrophages, as well as cell-intrinsic functions such as phagocytosis and fungicidal activities in neutrophils and BMMs (data not shown). Taken together, these results suggest that OPN is detrimental in an early stage of acute candidemia due to restricted emergency granulopoiesis.

Impact of OPN on MPPs at the single-cell level

Since MPPs consists of a small and highly defined population, we analyzed gene expression patterns of MPPs at the single-cell level. Twenty hours after thioglycollate injection, MPPs were flow-sorted from the BM of WT and *Spp1*$^{-/-}$ mice and submitted for single-cell sequencing (Supplementary Table 1). Dimensionality reduction indicated *Spp1*$^{-/-}$ MPPs to have distinct t-SNE plot distribution from WT MPPs (Supplementary Fig. 4a, b). Next, the two sets of data (WT and *Spp1*$^{-/-}$) were normalized by sequencing depth and overlaid on a t-SNE plot (Fig. 3a; Supplementary Fig. 4c), and generated ten distinct clusters (Fig. 3b; Supplementary Fig. 4d). Each cluster was dominated by either WT or *Spp1*$^{-/-}$ cells (Fig. 3c, d). Expression of *Birc5*, encoding survivin, was high in certain clusters, particularly ones consisting with *Spp1*$^{-/-}$ MPPs, such as clusters 1, 6, 7, and 8 (Fig. 3b, e).

Next, we sought to determine whether OPN negatively regulates myelopoiesis and increases lymphopoiesis by an *ex vivo* cell differentiation assay[33]. This assay is also single cell-based by plating one cell per well to observe the cell development into granulo-macrophage (GM) cells and/or B cells (Fig. 3f). Significantly more *Spp1*$^{-/-}$ MPPs included unipotent myeloid progenitors (‘GM only’ in Fig. 3g) than WT MPPs did. In addition, ‘plating efficiency’ (i.e., how many cells survived in the tissue culture) was high in *Spp1*$^{-/-}$ MPPs (Fig. 3h), reflecting high *Birc5* expression in *Spp1*$^{-/-}$ dominant clusters (Fig. 3e). The results also implicate better survival of MPPs without OPN.

OPN and apoptosis in myeloid vs. lymphoid progenitors

We asked how OPN inhibits emergency myelopoiesis. Gene expression levels of transcription factors (*Ikaros, Spi1, Notch1, Notch2, Gata2, Flt3, Pbx1, Scl, Hoxb3, Hoxb4*) critical for the developmental dichotomy from MPPs to either lymphoid and myeloid progenitors were comparable between WT and *Spp1*$^{-/-}$ MPPs after thioglycollate injection (Supplementary Fig. 4e). OPN also did not impact the proliferation of CMPs, GMPs and CLPs determined during emergency myelopoiesis induced by thioglycollate (Supplementary Fig. 5a, b). Therefore, we next examined if OPN affected apoptosis in the hematopoietic progenitors. At the steady-state, OPN had no impact on apoptosis of CMPs, GMPs, and CLPs (Supplementary Fig. 5c, d). However, in irradiation BM chimeras (Supplementary Fig. 5e), OPN significantly enhanced apoptosis in donor CMPs and GMPs, but not in CLPs (Fig. 4a, b). The similar pattern – OPN promotes apoptosis in CMPs and GMPs, but not CLPs – was observed in mice that had intraperitoneal thioglycollate injection (Fig. 4c, d) and systemic Candida infection (Fig. 4e). In contrast, apoptosis in differentiated myeloid cells,

such as neutrophils and monocytes, was not affected by OPN (Supplementary Fig. 5f, g), suggesting that the pro-apoptotic role of OPN is restricted to myeloid progenitors. As the *Birc5* transcript encoding survivin was identified in a single cell sequence analysis (Fig. 3e), enhanced expression of *Birc5* was also identified in GMPs from *Spp1*$^{-/-}$ mice 15 hr after Candida infection (Fig. 4f). Importantly, the expression of *Birc5* was not altered in CLPs, Gr-1^{+} cells and B cells in the BM (Fig. 4g; Supplementary Fig. 5h). Upregulation of survivin in *Spp1*$^{-/-}$ GMPs was also confirmed at the protein level (Fig. 4h).

Since OPN does not affect apoptosis in lymphoid progenitors (Fig. 4a–e), we examined whether differentiated lymphoid cells are affected by OPN. In the presence of OPN, apoptosis of T and B cells was inhibited in irradiation BM chimera (Fig. 4i, j). Even at steady state, apoptosis of B cells was slightly inhibited by OPN (Supplementary Fig. 5i). In contrast, OPN did not alter lymphocyte proliferation in irradiation BM chimera (Supplementary Fig. 5j, k). Thus, OPN plays an anti-apoptotic role in differentiated lymphoid cells in peripheral lymphoid organs. This result indicates a clear contrast in OPN's roles: OPN is pro-apoptotic in myeloid progenitors but anti-apoptotic in differentiated lymphoid cells.

Apoptosis of donor lymphocytes in lymphopenic recipients

Numbers and proportions of WT CD4^{+} T cells were significantly higher than those of *Spp1*$^{-/-}$ CD4^{+} T cells during chronic lymphopenia-induced proliferation (cLIP)[34], in which naive T cells were transferred to *Spp1*$^{-/-}$*Rag1*$^{-/-}$ (Fig. 5a, b). Despite comparable proliferation between WT and *Spp1*$^{-/-}$ donor CD4^{+} T cells (Fig. 5c, d), WT cells were less prone to apoptosis than *Spp1*$^{-/-}$ cells (Fig. 5e, f). We obtained similar results in transferred T cells in OPN-sufficient *Rag1*$^{-/-}$ recipients (Supplementary Fig. 6a–d), suggesting donor T cell-derived OPN protects T cells from apoptosis. Systemic OPN is determined by recipient-derived OPN (Supplementary Fig. 6e); thus, either T cell autocrine OPN or iOPN within T cells could in principle inhibit T cell survival.

Because T cell expansion in cLIP is mediated by gut commensal microbes[35], we first tested if CD4^{+} T cells from WT mice (*i.e.*, polyclonal) were proliferated *ex vivo* by total MLN cells without supplying exogenous antigens (Supplementary Fig. 6f). T cells were proliferated and survived better with MLN cells than those without MLN cells or with splenocytes (Supplementary Fig. 6g). In this *ex vivo* system, WT CD4^{+} T cells also proliferated better than *Spp1*$^{-/-}$ CD4^{+} T cells and were significantly protected from apoptosis, resulting in increased live and divided WT T cells (Fig. 5g–i). Importantly, the survival of *Spp1*$^{-/-}$ CD4^{+} T cells was recovered, at least partially, by supplying recombinant OPN (rOPN) in the cell culture (Fig. 5g, h), suggesting that anti-apoptotic function of OPN is mediated by sOPN. In contrast, OPN does not affect apoptosis and proliferation in T cells upon strong T cell receptor (TCR) stimulation with anti-CD3 plus CD28 antibodies (Supplementary Fig. 6h, i). These results indicated that sOPN supports T cell survival in activated T cells but not with strong TCR stimulation.

We also found that B cell-derived OPN significantly increased frequencies and numbers of B cells after being transferred into *Rag1*$^{-/-}$ lymphopenic recipients (Fig. 5j, k). Since B cells generally do not proliferate without T cells, this system without T cells evaluates B cell

survival rather than proliferation. Taken together, OPN expressed in T or B cells promote survival of the cells, and sOPN appears to be sufficient for the effect.

OPN exacerbates T cell-mediated colitis

Colitis was induced in *Rag1*$^{-/-}$ and *Spp1*$^{-/-}$*Rag1*$^{-/-}$ recipients by transferring CD62L^{hi}CD4^{+} T cells from naive WT and *Spp1*$^{-/-}$ mice. First, the involvement of OPN derived from donor and recipients was identified in recipient weight changes (Fig. 6a), but the following data indicated more impact of donor OPN than recipient OPN. The increase in colon weight per unit length, a sign of colitis severity, was mediated by WT donor T cells (Fig. 6b, c). Here, not only did WT T cells migrate to the colon more efficiently than *Spp1*$^{-/-}$ T cells, but WT myeloid cells also did (Fig. 6d). This phenotype entirely depended on OPN in donor T cells (Fig. 6d). With the presence of OPN in donor T cells, proportions of colon-infiltrated T helper subsets were skewed towards Th1 with reduced proportion of Tregs (Fig. 6e). Numbers of total cells and CD4^{+} T cells in the MLN also shared a similar trend as seen in the colon (Fig. 6f–h), as well as general increase in numbers of most of T helper subsets and myeloid cells in the colon with WT T cell transfer (Supplementary Fig. 6j, k). These results further linked donor T cell-derived OPN and severe pathological features of colitis, such as immune cell infiltration, thickened mucosal and submucosal layers, and disappearance of goblet cells (Fig. 6i). It is of note that OPN in donor T cells and recipients did not impact the expression of integrins, gut homing receptors, and T cell activation markers (Supplementary Fig. 6l, m). Taken together with the cLIP results, T cell-derived sOPN contributes to the T cell increase and significantly exacerbates colitis.

Ruling out the involvement of iOPN in lymphoid cell expansion

Activation of CD4^{+} T cells enhanced production of both sOPN and iOPN (Fig. 7a, b). Thus, we evaluated the involvement of iOPN by generating LSL-iOPN (LSL$^{fl/fl}$-*Δ45Spp1*; *Vav1*-cre) mice, which express iOPN but not sOPN, due to the deletion of the signal sequence (45-nt) that target OPN to secretory vesicles (Supplementary Fig. 7a). ES cell clones successfully expressing the target allele were determined by a Southern blot analysis, and the deletion of the signal sequence was confirmed in LSL-iOPN mice (Supplementary Fig. 7b, c). Levels of cytoplasmic iOPN separated by density gradient[23] in LSL-iOPN mice were comparable to those in WT mice (Supplementary Fig. 7d). Importantly, serum and cell culture supernatants of LSL-iOPN were free from OPN, *i.e.*, no sOPN (Supplementary Fig. 7e, f).

Using CD4^{+} T cells from the LSL-iOPN mice, we examined cLIP on day 6 (Fig. 7c, d) and day 28 (Fig. 7e). Numbers and proportions of CD4^{+} T cells were comparable between recipients which received *Spp1*$^{-/-}$ or LSL-iOPN T cells, but recipients with WT T cells showed more of the values (Fig. 7c–e), suggesting that sOPN enhances T cell expansion during cLIP. Furthermore, apoptosis between LSL-iOPN and *Spp1*$^{-/-}$ CD4^{+} T cells was similarly more frequent than WT CD4^{+} T cell apoptosis (Fig. 7f), again suggesting the involvement of sOPN. This result is also confirmatory to the *ex vivo* results demonstrating that sOPN, not iOPN, protected T cells from apoptosis (Fig. 5g, h). LSL-iOPN CD4^{+} T cells induced extremely mild colitis as *Spp1*$^{-/-}$ T cells did with low numbers of tissue-infiltrated cells and low histology scores, *e.g.*, well preserved goblet cells (Fig. 7g–i). The results

suggest that T cell iOPN is dispensable to induce OPN-dependent colitis. We also ruled out B cell iOPN in OPN-mediated B cell increase (Fig. 7j, k). In sum, sOPN is responsible for OPN-mediated lymphocyte survival and the resulting increase of lymphocyte population sizes.

Less myeloid cells by iOPN, more lymphoid cells by sOPN

Mixed BM radiation chimera were generated with LSL-iOPN and *Spp1*$^{-/-}$donor BM cells (Supplementary Fig. 2f, g). Three weeks after BM transfer, proportions of *Spp1*$^{-/-}$ MPPs, CMPs, and GMPs predominated over those of LSL-iOPN (Fig. 8a), indicating the involvement of iOPN in restricting the progenitor population sizes. Differentiated leukocytes were examined at 7 weeks after BM transfer. *Spp1*$^{-/-}$ cells were again predominant over LSL-iOPN cells for neutrophils and Ly6C^{+} monocytes/macrophages, not for T cells and B cells (Fig. 8b, c). When WT and LSL-iOPN BM cells were used as donors, no difference was observed in myeloid cell population sizes (Supplementary Fig. 8a–c), showing a clear contrast to WT and *Spp1*$^{-/-}$ mix BM chimera (Supplementary Fig. 8d). These data confirmed that iOPN restricts myeloid cell development by limiting myeloid progenitors, but not differentiated leukocytes, while sOPN expands lymphoid cells.

We further validated the impact of iOPN in myelopoiesis by an *ex vivo* single-cell progenitor differentiation assay (Fig. 8d). During emergency granulopoiesis induced by systemic Candida infection, iOPN (i.e., in WT and LSL-iOPN mice) decreased proportions and numbers of GMPs and neutrophils in the BM by enhanced apoptosis in CMPs and GMPs (Fig. 8e–h). Furthermore, iOPN enhanced activation of pan-caspases (predominantly caspase-1 and -3[36]) and reduced *Birc5* mRNA in GMPs (Fig. 8i, j). In sum, iOPN decreases myeloid cell populations, and sOPN increases lymphoid cell populations.

DISCUSSION

Previous reports showed that OPN decreased the pool size of LSK cells during the homeostatic state and after BM cell transplant[19, 20]. This study suggested that the function of OPN in GMPs and CMPs is quite distinct from that in LSK cells in the following points: (1) sOPN decreases LSK cells[19, 20] but iOPN decreases GMPs and CMPs; (2) the increase of LSK cells by OPN-deficiency does not affect population sizes of differentiated leukocytes[19, 20] but the increase of GMPs by iOPN-deficiency results in enlarged population sizes of myeloid cells during emergency myelopoiesis; and (3) non-hematopoietic stroma cells are the source of sOPN that decreases LSK cells but iOPN in the progenitor cells is attributed to the decrease of myeloid progenitors. Thus, although sOPN reduces population sizes of LSK cells, the mechanism by which iOPN reduces myeloid progenitors is quite different.

iOPN was detrimental during early Candida infection by limiting neutrophil supply. This may appear contradictory to a previous study demonstrating that iOPN protects hosts from Pneumocystis fungal infection[13]. However, major differences in these fungal infection models need to be noted. The previous Pneumocystis study focused on opportunistic and spontaneous infection in lymphopenic hosts and required 10–20 weeks to evaluate host mortality[13]. Under this long-term infection, emergency myelopoiesis most probably does not

apply. Therefore, iOPN appears to be either detrimental or beneficial, depending on timing and condition of a fungal infection.

A series of colitis studies strongly imply multifaceted roles of OPN. Some studies concluded that OPN induces immune responses[37, 38, 39], and others demonstrated that OPN suppresses immune responses[39, 40, 41]. One study provided an insightful suggestion that OPN suppresses immune responses during acute inflammation, but not in chronic inflammation[39]. In particular, sOPN was previously found to be attributable to chronic colitis[37, 39], and our data in this study is congruent with these findings.

sOPN's anti-apoptotic function was also demonstrated by others[42]. In contrast, the pro-apoptotic function of iOPN has not been reported in any cells. In this study, we demonstrated that iOPN enhances apoptosis in GMPs. We evaluated a possible involvement of p53 in inducing apoptosis by detecting phosphorylated p53, but no differences were found between WT and *Spp1* GMPs after Candida infection (data not shown). Instead, we found that OPN enhances apoptosis through the downregulation of survivin expression and enhancement of pan-caspase activities. Based on our single cell analysis result, it is possible that particular MPP subpopulations were paricularly regulated by iOPN to be advanced into myelopoiesis.

In this study, we dissected roles of sOPN and iOPN in shifting the balance of leukocyte populations during BM cell transplant after irradiation, fungal infection, and autoimmune colitis, and found differential regulation of myeloid vs. lymphoid cell populations by distinct OPN isoforms. Thus, iOPN and sOPN coordinately tip the balance of myeloid vs. lymphoid populations.

ONLINE METHODS

Animals and reagents

All the mice in this study were on the C57BL/6J background. *Spp1*$^{-/-}$ mice and *Vav1*-Cre mice were purchased from the Jackson Laboratory. LSL-iOPN mice were created in our laboratory with help from the Duke Transgenic Mouse Facility. Six- to eight-week old sex-matched WT, *Spp1*$^{-/-}$ and LSL-iOPN mice were used for all experiments. All the experiments were performed as approved by the Institutional Animal Care and Use Committee at Duke University, and all animals were housed under specific pathogen-free conditions. Readouts of *in vivo* disease model experiments were quantitatively determined by objective measurements; thus, blinding was not performed. The genotype of the ES cells and the mice was examined by Southern blot and PCR by using following probe and primers (Supplementary Fig. 7a–c). Probe for Southern blot: tcatttgcattcaatctgagcttgtcagacaaaattattcactttcattttatgagatttctctcatcaatacgcatataatgtagtctgcatacatgtggtagtctgcacacatgtggtagcctgcacacatagggtcgtatgcacacatggagtagtatcacacatgggataatatacccacatggggtagtgtgcacacatgtgttagtgtgtacacatgaggtagtgtgcacatatgttagtatgcatatgtgttaatatgtatagatggggtagtttgtacacatggggtagtatgcacacatgtgctatatacacacatgtgtgagtgtgcatacatggggtattatgcacatgtgttagtatgtacatatgggatagtgaacatacatggagtagtctacatacatgtgttagtatacacatatgtggaagccagaggacaagtccaggctttgttcctcctgcgttgtctatatatttttttgagacagggtctttcactggcctggaactcagcaaacaggctaaggcagacagagagtcctgagagtacaactgtctgtacctccccagtgctagaatgacaatgctgagcagt. Primers to detect deletion of

45 nucleotides in exon 2 of *Spp1* allele, forward: 5'-ACTTGGTGGTGATCTAGTGGTG-3', reverse: 5'-AGCAACCTTTGCGACGCTGGCGAAC-3'. Antibodies against CD45 (30-F11), CD45.1 (A20), CD45.2 (104), CD4 (GK1.5), CD3 (145-2C11), CD8 (53-6.7), Ly6G (1A8), Ly6C (HK1.4), CD11b (M1/70), CD11c (N418), CD49b (DX5), TER119 (TER-119), Gr-1 (RB6-8C5), B220 (RA3-6B2), CD19 (6D5), FcγR (93), CD34 (MEC14.7), IL-7R (A7R34), Flt3L (A2F10), Sca-1 (D7), c-kit (2B8), CD16/32 (93), E-cadherin (DECMA-1) and BrdU (Bu20a), G-CSF, GM-CSF were purchased from BioLegend. AMD3100 was purchased from Sigma. XMU-MP-1 was purchased from MedChem Express. To check LDH levels in the serum, Pierce™ LDH Cytotoxicity Assay Kit was used.

Tissue-infiltrated cell analyses by flow cytometry

Lung and liver tissues were cut into small pieces and incubated in a 1 mg/ml collagenase D solution at 37 °C for 30 min. Cells were then enriched by Percoll gradient (GE Healthcare). Followed by staining with specific antibodies, cells were analyzed with FACS Canto™ II (BD) and the FlowJo software (Treestar Inc.). For evaluation of apoptosis, FITC Annexin V Apoptosis Detection Kit with 7-AAD was used. Gating strategy is shown in Supplementary Fig. 1a, unless otherwise noted. Data on BM cell enumeration was enumerated per one tibia and one femur from one of the hind legs.

Real-time PCR and ELISA analysis

Total mRNA were reverse-transcribed to cDNA, and gene expression levels were determined by using the $-\Delta\Delta Ct$ method of real-time PCR as previously described[31, 43] by using primers shown in Supplementary Table 2. *Actb* expression was used as an internal control. For Fig. 2g, *Hsp90ab1* was used as an internal control. Results shown are representatives from multiple independent experiments with similar results. In Supplementary Fig. 3g, 4e, error bars (too short to be identified in Supplementary Fig. 3g) were drawn based on the calculation of RQ-Min = $2^{-(\Delta\Delta Ct + \mathrm{T} * \mathrm{SD}(\Delta Ct))}$ and RQ-Max = $2^{-(\Delta\Delta Ct - \mathrm{T} * \mathrm{SD}(\Delta Ct))}$ from triplicate wells as suggested by a manufacturer of PCR machines (Applied Biosystems). Error bars denote RQ-MIN and RQ-MAX, which constitute the acceptable error for a 95% confidence limit according to Student's t-test. ELISA for OPN was performed as previously described[44].

Experiments with Candida

Detailed methods for the experiments with Candida are described in our previous publication[45]. Candida infection was performed with sex-matched mice of age 6–8 week by intravenous (*i.v.*) injection of 2×10^6 spores of *Candida albicans* (ATCC 18804). Fifteen or twenty-four hour after Candida infection, cellularity and apoptotic cell ratio in the BM and spleen were examined by flow cytometry. Host cell phagocytosis of Candida spores was performed as follows. BMMs and thioglycollate-elicited neutrophils were co-cultured with Alexa Fluor 647 (AF647)-labeled Candida spores (host cells vs. spore ratio of 1:1) for 15, 30, 60 or 120 min. Host cells had been stained with antibodies against CD11b, F4/80 (for macrophages) or Ly6G (for neutrophils) before co-culture set up. Flow cytometry was used to determine cells phagocytosed Candida. For evaluating fungicidal activity by host cells, BMMs and thioglycollate-elicited neutrophils were used for the analyses were co-culture with live Candida with the 1:10 ratio (conidia : host)(termed "test samples") for 12 hours.

Negative control culture had Candida spores alone. Host cells were lysed with water, and Candida CFU was determined with YPD plates. Results were obtained with the following formula: Candida Expansion (fold) = [CFU at 12 hrs]/[CFU at 0-h]; Inhibition of Candida expansion (%) = (1 − [CFU of test samples at 12 hrs]/[CFU of negative control at 12 hrs]) × 100.

Treating mice with Thioglycollate or AMD3100

WT or *Spp1*$^{-/-}$ mice were intraperitoneally injected with 3% thioglycollate (2.5 ml per mouse) or AMD3100 (5 mg/kg mouse weight). GMPs were sorted from BM of the mice at 0, 6, 12, 24 or 48 after the treatment. *Spp1* expression in the cells was examined by qPCR. Cell numbers and PMN frequencies were calculated from flow cytometry data.

Ex vivo single-cell MPP differentiation assay

To analyze the differentiation potential of MMPs, single MPP cells were sorted by MoFlo XDP (Beckman Coulter) and plated (one cell/well) in the MEM alpha (Life technology) medium containing 20% ES cell-grade FBS (Millipore), SCF (50 ng/ml: BioLegend), and Flt3 ligand (30 ng/ml: BioLegend) on the layer of OP9 cells in 96-well plates as previously described[33]. The OP9 cell line was obtained from ATCC and confirmed to be free of mycoplasma by using the MycoAlert PLUS kit (Lonza). Two days after cell plating, IL-3 (10 ng/ml; BioLegend), IL-7 (10 ng/ml; BioLegend), and GM-CSF (10 ng/ml; R&D Systems) were added to each well to induce cell differentiation. “Plating efficiency” denotes cells successfully expanded in culture, determined by microscopic observation. Expanded cells were analyzed by flow cytometry to determine whether they developed into either granulocyte/macrophages (GM) (Gr-1^{+}CD11b^{+}B220^{-}CD19^{-} and Gr-1^{-}CD11b^{+}B220^{-}CD19^{-}) or B cells (Gr-1^{-}CD11b^{-}B220^{+}CD19^{+}).

Separating of cytoplasmic proteins

Separation was performed by two methods. One is by using NE-PER™ Nuclear and Cytoplasmic Extraction Reagents, as instructed by the supplier (Pierce). Another is by the density gradients. In the latter method, tissues from WT, *Spp1*$^{-/-}$ and LSL-iOPN mice were homogenized in the homogenization medium (0.25 M sucrose, 1mM EDTA 10 mM Hepes-NaOH, pH 7.4), then mixed with iodixanol as the final concentration of 30%. Homogenates in 30% iodixanol solution (1125 μl) were placed at the bottom, then layered with 25% (w/v) of iodixanol solution (2 ml) in the middle and 5% (w/v) iodixanol solution (2 ml) on the top. Using the Beckman Ultracentrifuge L9 and Beckman SW40.1 rotor, samples were centrifuged at 35,000rpm (250,000g) at 4 °C for 3 hr. Eight layers fractions were carefully collected from the top to the bottom by pipette. Cytoplasmic compartments were identified by Western blotting. Separation of the cytoplasmic proteins was confirmed by detecting GAPDH, but not calnexin. The cytoplasmic fractions were used to evaluate the iOPN expression.

Cell proliferation analysis

To analyze cell proliferation *in vivo*, BrdU (10 ml/kg) (Invitrogen) was intraperitoneally injected into mice. Twenty-four hour after the injection, cells obtained from the spleen or

BM. After fixation with 2% PFA, permeabilization with 0.5% Triton X-100 in PBS, cells were treated with RQ1 RNase-Free DNase (Promega). With BrdU antibody, cells were stained, then BrdU incorporation was analyzed by flow cytometry. For experiments shown in Supplementary Fig. 3c, cell proliferation was evaluated by Ki-67 staining. BM cells were harvested and stained for cell surface markers, fixed, and permeabilized by incubating with cold 70% ethanol at −20°C for 1hr. Then, cells were stained with anti-Ki-67 antibody and analyzed by flow cytometry.

Generation of mix BM chimera mice

Mix WT-*Spp1*$^{-/-}$ BM chimera mice were generated by adoptively transferring 5×10^6 each of BM cells obtained from naive WT mice (CD45.1/CD45.2) and *Spp1*$^{-/-}$ mice (CD45.2) to lethally irradiated (900 rad) WT mice (CD45.1), as shown Supplementary Fig. 2a. For LSK cell chimera mice, 10^4 each of LSK cells isolated from WT (CD45.1) and *Spp1*$^{-/-}$ mice (CD45.2) were adoptively transferred to lethally irradiated (900 rad) WT mice (CD45.1/CD45.2) with 10^7 of c-kit$^-$ BM cells, as "rescue cells," obtained from WT mice (CD45.1/CD45.2). Other mix BM chimera mice were also prepared similarly. Ratios between mixed donor cells were analyzed 3, 6, or 7 weeks after BM cell transfer by flow cytometry. The methods were also depicted in Supplementary Fig. 2.

Lymphopenia-induced lymphocyte proliferation and T cell-induced colitis

CD62L^{hi}CD4$^+$ T cells (10^6/ mouse) were intravenously injected to *Rag1*$^{-/-}$ or *Rag1*$^{-/-}$*Spp1*$^{-/-}$ mice. Donor T cell apoptosis and population sizes were examined at day 3 and/or 6. The severity of colitis was evaluated by the ratio between weight and length of the colon, as well as histology staining with H&E and Alcian blue, at 4 weeks after T cell transfer. Histological scoring was performed as previously described[46]. Colon infiltrated cells were isolated by using Lamina Propria Dissociation Kit (Miltenyi Biotec). To evaluate T cell proliferation, donor T cells were labeled with CellTrace Violet (Thermo Fisher Scientific inc.), and evaluated by flow cytometry 6 days after the injection. To examine an impact of OPN in maintaining B cell population, B cells (2× 10^6/ mouse) were adoptively transferred to *Rag1*$^{-/-}$ and analyzed the population size by flow cytometry at 4 weeks after the cell transfer.

Ex vivo T cell proliferation assay

Total MLN cells obtained from *Rag1*$^{-/-}$ or *Rag1*$^{-/-}$*Spp1*$^{-/-}$ mice were co-cultured with WT or *Spp1*$^{-/-}$ CFSE-labeled CD62L^{hi}CD4$^+$ T cells at the 1:1 ratio in the absence or presence of neutralizing OPN antibody (AF808: 10 μg/ml) for 7 days. Cell proliferation and cell death were evaluated by dilution of CFSE (or CellTrave Violet) and LIVE/DEAD staining, respectively. In some experiment, CD62L^{hi}CD4$^+$ T cells obtained from WT or *Spp1*$^{-/-}$ mice were labeled with CellTrace Violet and stimulated with Dynabeads T-Activator CD3/CD28 (TermoFisher Scientific). T cell apoptosis was examined by 7-AAD staining.

Single-cell RNA sequencing

MPPs were flow-sorted as Lin$^-$Sca-1$^+$c-kit$^+$CD34$^+$Flt3L$^+$ from BM of WT and *Spp1*$^{-/-}$ mice 20 hrs after thioglycollate intraperitoneal injection and submitted for single-cell

sequencing. For *10x Transcriptome library prep*, flow-sorted MPPs were resuspended in a 1× PBS / 0.04% BSA solution, at a concentration of 1000 cells/μl. After size selection (<50 μm), the cell suspensions were washed with a 1× PBS / 0.04% BSA solution to remove debris, clumps, dead cells and contaminants, and a cell counter used to determine the cell concentration and the solution normalized to 1×10^6 cells/ml. Cell preps were titrated to contain ~3000 cells per library. Cells were then combined with a master mix that contains reverse transcription reagents, and combined on the 10X instrument (10X Genomics, Inc., Pleasanton, CA) with gel beads carrying the Illumina P7 and R2 primers, a 14-bp identifying barcode, a 10-bp randomer for RNA molecule quantitation, and a poly-dT primer, and oil for the emulsion PCR. Cells were partitioned into nanoliter-scale gel beads in emulsion (GEMS) within which reverse-transcription is carried out and all cDNAs within a GEM, *i.e.* from one cell, share a common barcode. After the RT reaction, the GEMs are/were broken and the full-length cDNAs cleaned with both Silane Dynabeads (Thermo Fisher Scientific, Waltham, MA) and SPRI beads (Beckman Coulter Life Sciences, Indianapolis IN). After purification, the cDNAs were run on the Agilent Bioanalyzer High Sensitivity chip (Agilent Technologies, Santa Clara, CA) for qualitative analysis. cDNA in single cells was sheared to ~200-bp with a Covaris S220 Focused-ultrasonicator (Covaris, Inc., Woburn, MA) and then sequencing libraries constructed for running on an Illumina high-throughput sequencer. This entailed end repair and A-tailing, P5 adapter ligation, SPRI bead clean-up, a sample index PCR, and further SPRI bead clean-ups. The sample index PCR adds a unique sample index for sample multiplexing during sequencing, with P5 and P7 primers used in Illumina bridge amplification. The sequence was generated using 125-bp paired-end sequencing on an Illumina 2500 sequencing platform (Illumina, Inc., San Diego, CA) at the David H Murdock Research Institute (Kannapolis, NC). Supplementary Table 1 shows the cell count and sequencing totals, including unique molecular identifiers which allow for within cell, gene specific counts of RNA molecules.

Single cell sequence cell data analysis

The primary analytical pipeline for the SC data followed the recommended protocols from 10X Genomics. Briefly, raw FASTQ files were processed using Cell Ranger software (v 1.1) to first demultiplex the raw reads and align the reads to the mouse transcriptome. PCR duplicates were flagged, non-cellular reads filtered out, and gene expression matrices created for all single cells in each sample (http://support.10xgenomics.com/single-cell/software/pipelines/latest/what-is-cell-ranger). We performed a secondary analysis using an R statistical methodology, R package Seurat (http://satijalab.org/seurat/). Samples were normalized based on sequencing depth, then combined into a single gene expression matrix in Cell Ranger. In Seurat, the combined expression matrix was normalized on the log scale after basic filtering for minimum gene and cell observance frequency cut-offs (http://satijalab.org/seurat/pbmc-tutorial.html). We then closely examined the data and performed further filtering based a range of metrics in an attempt to identify and exclude possible multiplets (i.e. instances where more than one cell was present and sequenced in an emulsified gel bead). After quality control procedures had completed, we calculated principal components using the most variably expressed genes in the dataset. Significant principal components for downstream analyses were determined through methods mirroring those implemented by Macosko et al[47], and these principal components were carried

forward to perform cell clustering and enhance visualization (http://satijalab.org/seurat/pbmc-tutorial.html). Cells were grouped into an optimal number of clusters using Seurat's FindClusters() function, with visualization of cells being achieved through the use of t-SNE, which reduces the information captured in the selected significant principal components to two dimensions. Additional downstream analyses included examining the cellular distribution of *a priori* genes of interest, and closer examination of genes associated with cell clusters.

Statistical analysis

Statistical analysis was evaluated by using Microsoft Excel or Prism software version 3.02 (GraphPad). The two-tailed Student's t-test was used for statistical analyses of two-group comparisons. Multigroup comparisons were performed by a one-way analysis of variance (ANOVA) followed by Tukey–Kramer multiple comparisons test. In Fig. 2k, 3d, 3g and 8d, Chi-square test was used to determine if there is a significant relationship between two categorical variables. χ^2 statistics were derived using the CHIDIST function of Microsoft Excel. The criterion of significance was set at $p<0.05$. All results are expressed as mean ± SEM. Blinding or randomization to the groups were not performed and no data points were excluded for analyses. No statistical methods were used to predetermine to justify sample sizes, but our sample sizes are similar to those generally employed in the field.

Supplementary Material

Refer to Web version on PubMed Central for supplementary material.

Acknowledgments

We thank Dr. M. Ciofani for and Mr. M. Zuberbuehler (Department of Immunology, Duke University) for helping an experiment with fetal liver, Dr. M. Kondo (Toho University, Japan) for analysis of *ex vivo* progenitor differentiation assays, and Mr. Gary Kucera (Duke University) for generating the LSL-iOPN BAC construct. We would also like to thank the staff at the David H Murdock Research Institute for generating the sequence data, Ms. Karen Abramson and Ms. Emily Grass (Molecular Genomics Core, Duke Molecular Physiology Institute) for generating the 10X single cell libraries, and Ms. T. Kadota (Duke University) for helping *in vitro* experiments with BMMs in this study. This work was supported by the National Institutes of Health (R01AI088100 and R21AI103584 to M.L.S.) and U.S. Department of Defense (PC100266 to M.L.S.).

References

1. Manz MG, Boettcher S. Emergency granulopoiesis. Nat Rev Immunol. 2014; 14:302–314. [PubMed: 24751955]
2. Takizawa H, Boettcher S, Manz MG. Demand-adapted regulation of early hematopoiesis in infection and inflammation. Blood. 2012; 119:2991–3002. [PubMed: 22246037]
3. Patchen ML, MacVittie TJ, Williams JL, Schwartz GN, Souza LM. Administration of interleukin-6 stimulates multilineage hematopoiesis and accelerates recovery from radiation-induced hematopoietic depression. Blood. 1991; 77:472–480. [PubMed: 1991164]
4. Boettcher S, Manz MG. Regulation of Inflammation- and Infection-Driven Hematopoiesis. Trends Immunol. 2017
5. Lieschke GJ, et al. Mice lacking granulocyte colony-stimulating factor have chronic neutropenia, granulocyte and macrophage progenitor cell deficiency, and impaired neutrophil mobilization. Blood. 1994; 84:1737–1746. [PubMed: 7521686]

6. Zhan Y, Cheers C. Haemopoiesis in mice genetically lacking granulocyte-macrophage colony stimulating factor during chronic infection with Mycobacterium avium. Immunol Cell Biol. 2000; 78:118–123. [PubMed: 10762411]
7. Bernad A, et al. Interleukin-6 is required in vivo for the regulation of stem cells and committed progenitors of the hematopoietic system. Immunity. 1994; 1:725–731. [PubMed: 7895162]
8. Zhan Y, Lieschke GJ, Grail D, Dunn AR, Cheers C. Essential roles for granulocyte-macrophage colony-stimulating factor (GM-CSF) and G-CSF in the sustained hematopoietic response of Listeria monocytogenes-infected mice. Blood. 1998; 91:863–869. [PubMed: 9446646]
9. Bugl S, et al. Steady-state neutrophil homeostasis is dependent on TLR4/TRIF signaling. Blood. 2013; 121:723–733. [PubMed: 23223360]
10. Cain DW, Snowden PB, Sempowski GD, Kelsoe G. Inflammation triggers emergency granulopoiesis through a density-dependent feedback mechanism. PLoS One. 2011; 6:e19957. [PubMed: 21655273]
11. Inoue M, et al. T cells down-regulate macrophage TNF production by IRAK1-mediated IL-10 expression and control innate hyperinflammation. Proc Natl Acad Sci U S A. 2014; 111:5295–5300. [PubMed: 24706909]
12. Shinohara ML, Kim JH, Garcia VA, Cantor H. Engagement of the type I interferon receptor on dendritic cells inhibits T helper 17 cell development: role of intracellular osteopontin. Immunity. 2008; 29:68–78. [PubMed: 18619869]
13. Inoue M, et al. Cutting edge: critical role of intracellular osteopontin in antifungal innate immune responses. J Immunol. 2011; 186:19–23. [PubMed: 21135164]
14. Leavenworth JW, Verbinnen B, Wang Q, Shen E, Cantor H. Intracellular osteopontin regulates homeostasis and function of natural killer cells. Proc Natl Acad Sci U S A. 2015; 112:494–499. [PubMed: 25550515]
15. Rittling SR, Singh R. Osteopontin in Immune-mediated Diseases. J Dent Res. 2015; 94:1638–1645. [PubMed: 26341976]
16. Uede T. Osteopontin, intrinsic tissue regulator of intractable inflammatory diseases. Pathol Int. 2011; 61:265–280. [PubMed: 21501293]
17. Shevde LA, Samant RS. Role of osteopontin in the pathophysiology of cancer. Matrix Biol. 2014; 37:131–141. [PubMed: 24657887]
18. Kreke MR, Huckle WR, Goldstein AS. Fluid flow stimulates expression of osteopontin and bone sialoprotein by bone marrow stromal cells in a temporally dependent manner. Bone. 2005; 36:1047–1055. [PubMed: 15869916]
19. Stier S, et al. Osteopontin is a hematopoietic stem cell niche component that negatively regulates stem cell pool size. J Exp Med. 2005; 201:1781–1791. [PubMed: 15928197]
20. Nilsson SK, et al. Osteopontin, a key component of the hematopoietic stem cell niche and regulator of primitive hematopoietic progenitor cells. Blood. 2005; 106:1232–1239. [PubMed: 15845900]
21. Grassinger J, et al. Thrombin-cleaved osteopontin regulates hemopoietic stem and progenitor cell functions through interactions with alpha9beta1 and alpha4beta1 integrins. Blood. 2009; 114:49–59. [PubMed: 19417209]
22. Inoue M, Shinohara ML. Intracellular osteopontin (iOPN) and immunity. Immunol Res. 2011; 49:160–172. [PubMed: 21136203]
23. Shinohara ML, Kim HJ, Kim JH, Garcia VA, Cantor H. Alternative translation of osteopontin generates intracellular and secreted isoforms that mediate distinct biological activities in dendritic cells. Proc Natl Acad Sci U S A. 2008; 105:7235–7239. [PubMed: 18480255]
24. Leavenworth JW, Verbinnen B, Yin J, Huang H, Cantor H. A p85alpha-osteopontin axis couples the receptor ICOS to sustained Bcl-6 expression by follicular helper and regulatory T cells. Nat Immunol. 2015; 16:96–106. [PubMed: 25436971]
25. Shinohara ML, et al. Osteopontin expression is essential for interferon-alpha production by plasmacytoid dendritic cells. Nat Immunol. 2006; 7:498–506. [PubMed: 16604075]
26. Ashkar S, et al. Eta-1 (osteopontin): an early component of type-1 (cell-mediated) immunity. Science. 2000; 287:860–864. [PubMed: 10657301]
27. Sekido Y. Molecular pathogenesis of malignant mesothelioma. Carcinogenesis. 2013; 34:1413–1419. [PubMed: 23677068]

28. Robinson BS, Moberg KH. Cell-cell junctions: alpha-catenin and E-cadherin help fence in Yap1. Curr Biol. 2011; 21:R890–892. [PubMed: 22075429]
29. Kim NG, Koh E, Chen X, Gumbiner BM. E-cadherin mediates contact inhibition of proliferation through Hippo signaling-pathway components. Proc Natl Acad Sci U S A. 2011; 108:11930–11935. [PubMed: 21730131]
30. Qin F, Tian J, Zhou D, Chen L. Mst1 and Mst2 kinases: regulations and diseases. Cell Biosci. 2013; 3:31. [PubMed: 23985272]
31. Kanayama M, et al. Autophagy enhances NFkappaB activity in specific tissue macrophages by sequestering A20 to boost antifungal immunity. Nat Commun. 2015; 6:5779. [PubMed: 25609235]
32. Basu S, et al. "Emergency" granulopoiesis in G-CSF-deficient mice in response to Candida albicans infection. Blood. 2000; 95:3725–3733. [PubMed: 10845903]
33. Lai AY, Lin SM, Kondo M. Heterogeneity of Flt3-expressing multipotent progenitors in mouse bone marrow. J Immunol. 2005; 175:5016–5023. [PubMed: 16210604]
34. Surh CD, Sprent J. Homeostasis of naive and memory T cells. Immunity. 2008; 29:848–862. [PubMed: 19100699]
35. Kieper WC, et al. Recent immune status determines the source of antigens that drive homeostatic T cell expansion. J Immunol. 2005; 174:3158–3163. [PubMed: 15749843]
36. Yang B, et al. Inhibitors directed towards caspase-1 and-3 are less effective than pan caspase inhibition in preventing renal proximal tubular cell apoptosis. Nephron Exp Nephrol. 2004; 96:e39–51. [PubMed: 14988591]
37. Kourepini E, et al. Osteopontin expression by CD103- dendritic cells drives intestinal inflammation. Proc Natl Acad Sci U S A. 2014; 111:E856–865. [PubMed: 24550510]
38. Oz HS, Zhong J, de Villiers WJ. Osteopontin ablation attenuates progression of colitis in TNBS model. Dig Dis Sci. 2012; 57:1554–1561. [PubMed: 22173746]
39. Heilmann K, et al. Osteopontin as two-sided mediator of intestinal inflammation. J Cell Mol Med. 2009; 13:1162–1174. [PubMed: 18627421]
40. Toyonaga T, et al. Osteopontin Deficiency Accelerates Spontaneous Colitis in Mice with Disrupted Gut Microbiota and Macrophage Phagocytic Activity. PLoS One. 2015; 10:e0135552. [PubMed: 26274807]
41. Da Silva AP, et al. Exacerbated tissue destruction in DSS-induced acute colitis of OPN-null mice is associated with downregulation of TNF-alpha expression and non-programmed cell death. J Cell Physiol. 2006; 208:629–639. [PubMed: 16741956]
42. Hur EM, et al. Osteopontin-induced relapse and progression of autoimmune brain disease through enhanced survival of activated T cells. Nat Immunol. 2007; 8:74–83. [PubMed: 17143274]
43. Kanayama M, He YW, Shinohara ML. The lung is protected from spontaneous inflammation by autophagy in myeloid cells. J Immunol. 2015; 194:5465–5471. [PubMed: 25911758]
44. Shinohara ML, et al. T-bet-dependent expression of osteopontin contributes to T cell polarization. Proc Natl Acad Sci U S A. 2005; 102:17101–17106. [PubMed: 16286640]
45. Kanayama M, et al. Autophagy enhances NFkappaB activity in specific tissue macrophages by sequestering A20 to boost antifungal immunity. Nat Commun. 2015; 6:5779. [PubMed: 25609235]
46. Chinen T, et al. Prostaglandin E2 and SOCS1 have a role in intestinal immune tolerance. Nat Commun. 2011; 2:190. [PubMed: 21304519]
47. Macosko EZ, et al. Highly Parallel Genome-wide Expression Profiling of Individual Cells Using Nanoliter Droplets. Cell. 2015; 161:1202–1214. [PubMed: 26000488]

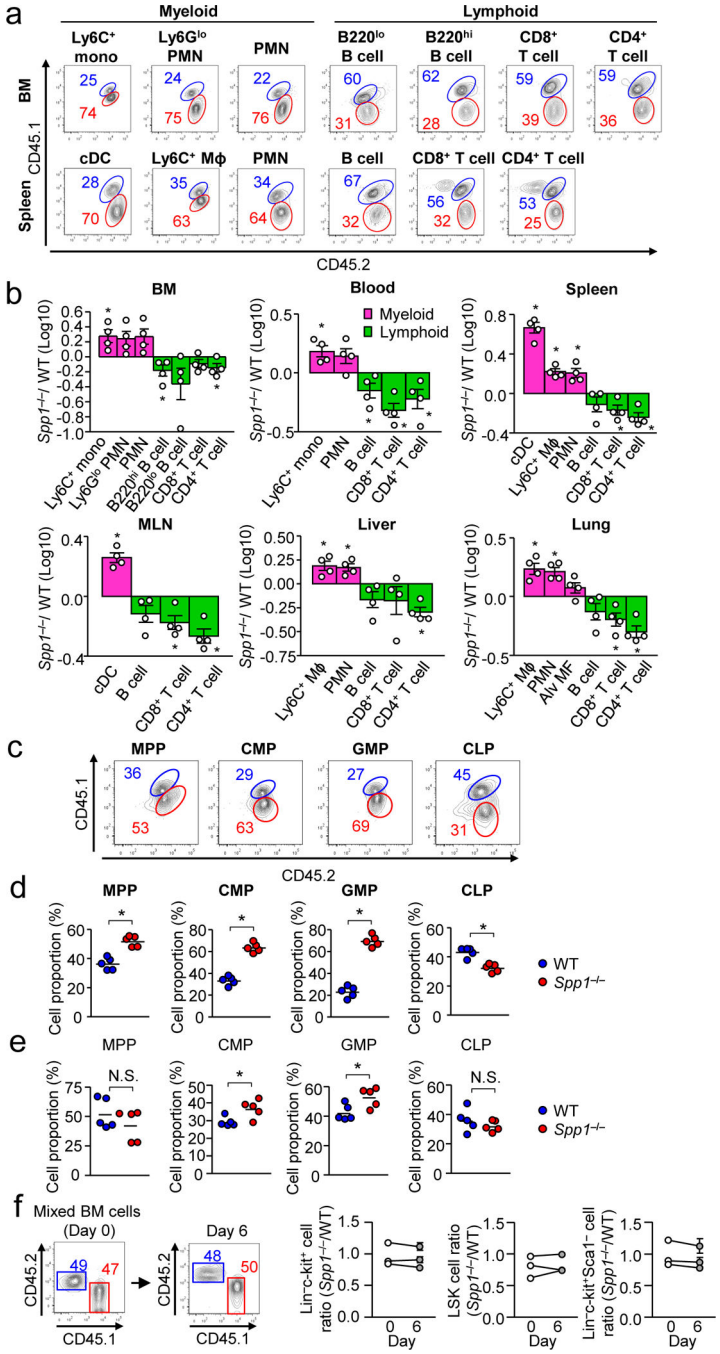

Figure 1. Analysis of cell population in irradiation mix BM chimera mice generated with WT vs. *Spp1*$^{-/-}$ donor cells

WT (CD45.1/CD45.2) and *Spp1*$^{-/-}$ mice (CD45.2) to irradiated WT recipients (CD45.1). **(a)** Flow cytometry to detect indicated cell populations of WT (labeled with blue) and *Spp1*$^{-/-}$ (labeled with red) donor origins in the BM and spleens 7-wk after BM cell transfer. **(b)** Ratios (*Spp1*$^{-/-}$/WT) of donor cell numbers in the indicated organs. Mϕ: macrophages. Datasets are representative of two independent experiments. (**c, d**) Analyzing hematopoietic progenitors in the BM of the mixed BM-chimera mice at 3 weeks after BM transplantation.

Representative flow plots (c) and frequencies of WT and *Spp1*$^{-/-}$ cells in indicated progenitors (d). (**e**) Instead of total BM cells, LSK cells from WT (CD45.1) and *Spp1*$^{-/-}$ (CD45.2) were transferred to WT recipients (CD45.1/CD45.2). Ratios of WT and *Spp1*$^{-/-}$ progenitor cells were assessed by flow cytometry at 3 weeks after transfer. Each dataset is a representative of two independent repeats (5 mice per group)(c–e). (**f**) Equal numbers of BM cells from naive WT (CD45.2) and *Spp1*$^{-/-}$ (CD45.1) mice were transferred to irradiated WT recipients (CD45.1/CD45.2). Six days after BM cell transfer, the ratio of WT and *Spp1*$^{-/-}$ in Lin^{-}c-kit^{+}, LSK (Lin^{-}Sca-1^{+}c-kit^{+}), and Lin^{-}Sca-1^{+}c-kit^{-} cells in the BM was examined. $n=3$ per each circle on day 6. Data were from three independent experiments. Error bars indicate ± SEM. * $p<0.05$ (Student's t-Test).

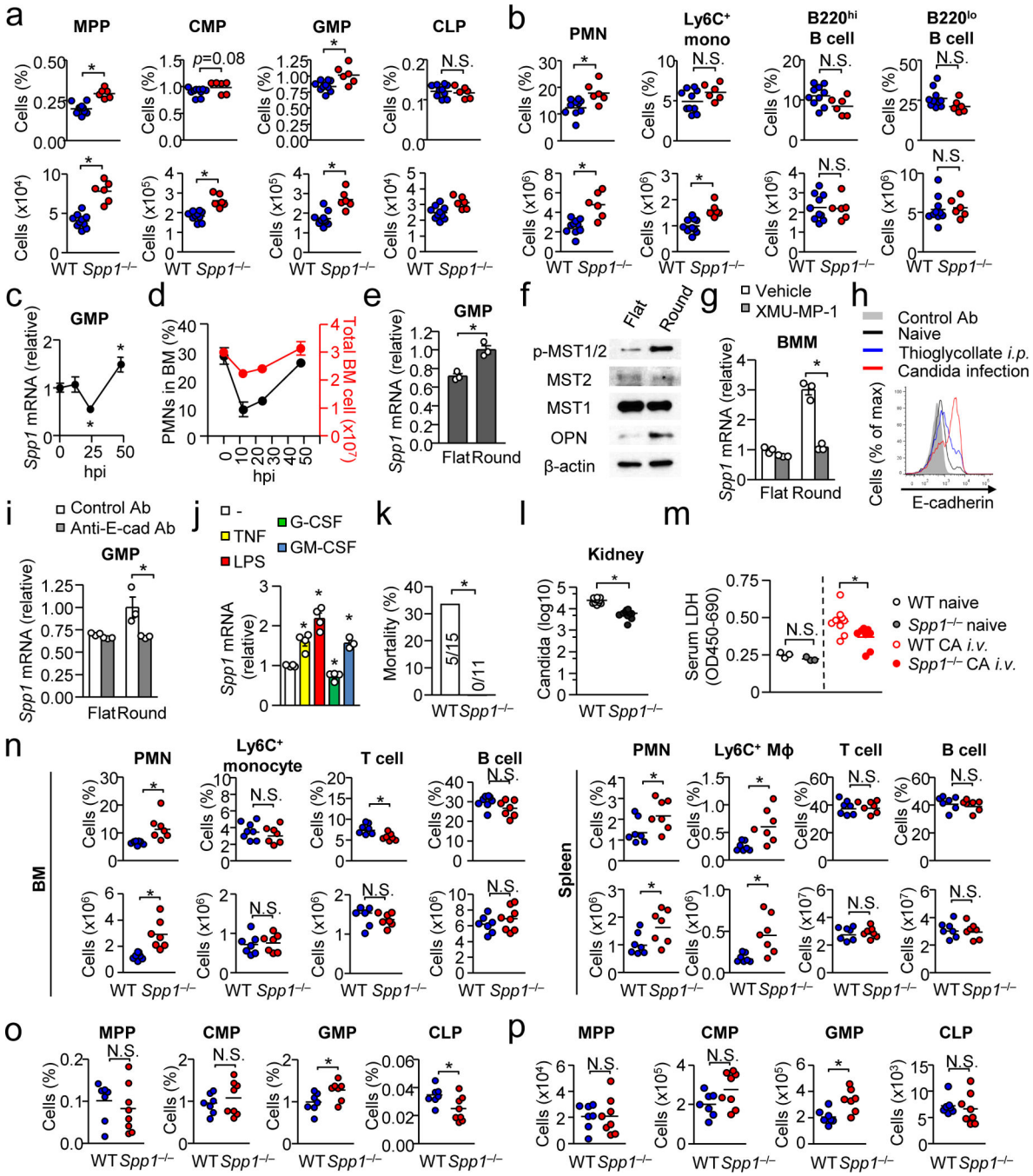

Figure 2. OPN inhibits emergency myelopoiesis

(**a, b**) Proportions and numbers of indicated progenitors (a) and differentiated cell subsets (b) in the BM 24 hrs after thioglycollate *i.p.* injection. Data were pooled from two independent experiments with 3–5 mice per experiment. (**c**) *Spp1* (OPN) mRNA levels in GMPs from BM of WT mice at indicated time points. hpi: hrs post injection. *n=4* per group. (**d**) Total cell numbers and frequency of neutrophils in the BM after thioglycollate *i.p.* injection. *n=4* per group. (**e**) *Spp1* mRNA levels in GMPs at 16 hrs after starting cell culture in flat- vs. round-bottom plates. (**f**) Western blotting of lysates of BMMs cultured in flat- or

round-bottom wells for 12 hr. (**g**) Reduction of *Spp1* expression by inhibiting MST1/2. BMMs were cultured on flat- or round-bottom plates (10^5 per well) with or without an Mst1/2 inhibitor (XMU-MP-1; 5 μg/ml). (**h**) E-cadherin expression levels on GMPs, which were harvested at 0 or 24 hr from WT mice after thioglycollate *i.p.* injection and Candida infection. (**i**) Reduction of *Spp1* mRNA by blockade of E-cadherin. Similar setting to (g) but GMPs and anti-E-cadherin antibody (10 μg/ml) were used. (**j**) *Spp1* mRNA levels in GMPs stimulated with TNF-α, LPS, G-CSF and GM-CSF (10 ng/ml for all) for 6 hrs in flat- or round-bottom wells. Datasets are representative of two (d–j) or three (c) independent experiments. (**k**) Mortality of *mice i.v.*-injected with 2×10^6 *Candida albicans* spores at 24 hrs after infection. Data were pooled from three independent experiments. (**l**) Candida CFU in the kidney 24 hrs after *i.v.*-injecting Candida spores (10^6 spores/mouse). (**m, n**) Comparison of serum levels of lactate dehydrogenase (LDH), indicating tissue damage (m), and cell numbers and frequencies in the BM and spleen 24 hrs after systemic Candida infection (n). (**o, p**) Proportions (o) and numbers (p) of BM progenitors during at 15 hrs after Candida infection. Error bars indicate ± SEM (c–e, g, i, j). * $p<0.05$. N.S.; not significant. Data were analyzed by the Student's t-test (a, b, c, e, g, i, j, l–p) or by the Chi-square test (k).

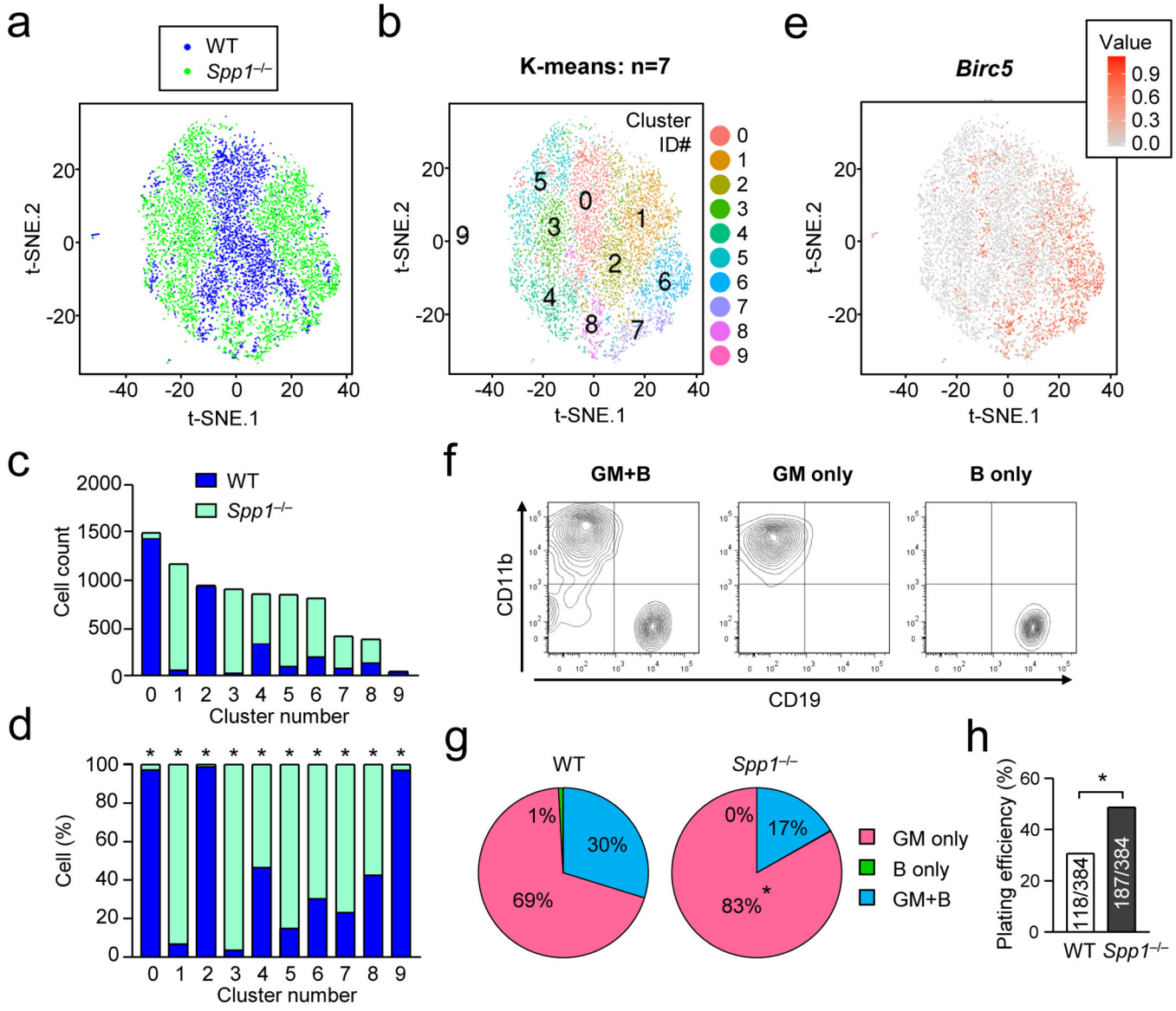

Figure 3. Single cell sequencing and *Ex vivo* MPP differentiation assay

(**a–f**) Single-cell RNA sequencing of MPPs from BMs of WT and *Spp1*$^{-/-}$ mice 20 hrs after intraperitoneal injection of thioglycollate. Numbers of sequenced MPPs of WT and *Spp1*$^{-/-}$ are 3,294 and 4,574, respectively. Two sets of data from WT (blue) and *Spp1*$^{-/-}$ (green) MPPs were normalized by sequencing depth and analysis of batch effects visualized by reduction to 2D by PCA and t-distributed stochastic neighbor embedding (t-SNE) plot (a). The cells in the t-SNE plot in (a) were clustered as K-means of 10 (b). Numbers in (b) denote cluster ID. Numbers of WT and *Spp1*$^{-/-}$ MPPs in each cluster in (b) are shown in (c). Ratios of WT and *Spp1*$^{-/-}$ cells in each cluster are shown in (d). *Birc5* mRNA expression levels in single cells are indicated (e). (**f–h**) *Ex vivo* single-cell MPP differentiation assay. Representative flow plots showing the MPP development to granulocyte-myeloid (GM) and B cells both (“GM+B”, left panel), GM cells (middle), and B cells (right)(f). Percentages of MPPs developed into the indicated cell types (g). Plating efficiency of WT and *Spp1*$^{-/-}$

MPPs denotes percentages of wells that included proliferated and survived cells at the time of cell harvest (h). Data are representative of two independent experiments. * $p<0.05$. Data were analyzed by the Chi-squared test (c, d, h).

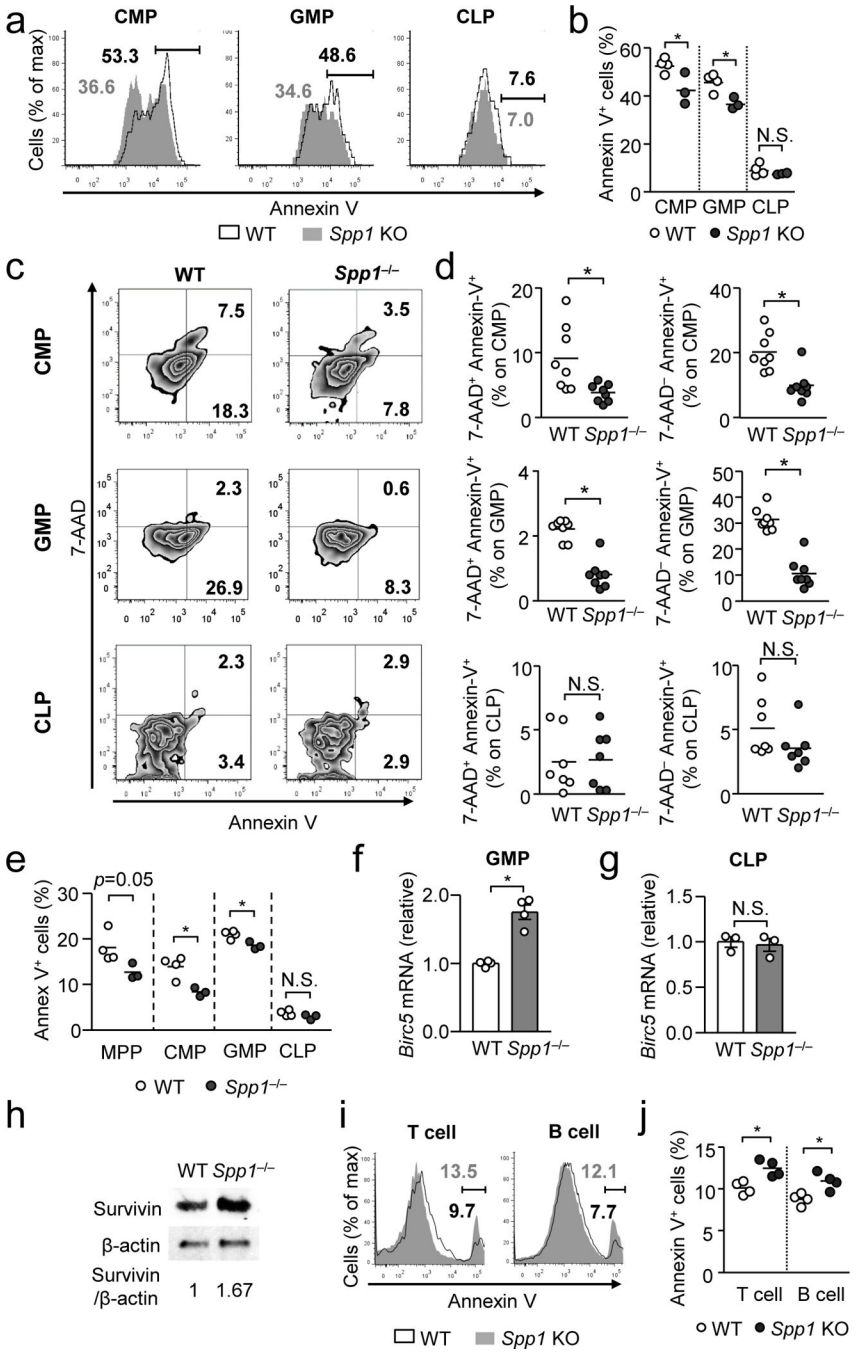

Figure 4. OPN plays opposing roles in apoptosis of myeloid progenitors and lymphoid cells

(**a, b**) Annexin-V staining of indicated progenitors at 3 weeks after BM cell transfer (WT or *Spp1−/−*) to WT recipients, as shown in Supplementary Fig. 5e. Representative flow panels (a) and data from a single experiment from two independent experiments. One circle denotes data from one recipient mouse. (**c, d**) Annexin-V and 7-AAD staining in indicated progenitors in the BM at 24 hrs after *i.p.* thioglycollate injection (not BM chimera). Representative flow plots (c) and data pooled from two independent experiments (d) are shown. (**e**) Apoptotic progenitors 15-hrs after systemic Candida infection (2×10^6 spores/

mouse) in BM of WT and *Spp1*$^{-/-}$ mice (not BM chimera). (**f, g**) *Birc5* mRNA levels of in GMPs (**f**) and CLPs (**g**) 15 hr after systemic Candida infection (2×10^6 spores/mouse). (**h**) A representative Western image of survivin expression in GMPs 15 hr after Candida infection (left). Survivin expression levels normalized β-actin expression (right). (**i, j**) Annexin-V staining of lymphoid cells in the spleen of recipients described in (a, b). Representative histograms (i) and frequencies of Annexin-V$^+$ T and B cells (j) are shown. Data are representatives of independent two (a, b, e–j) or three (c, d) experiments. Error bars denote ± SEM. * $p<0.05$ (Student's t-Test). N.S.; not significant.

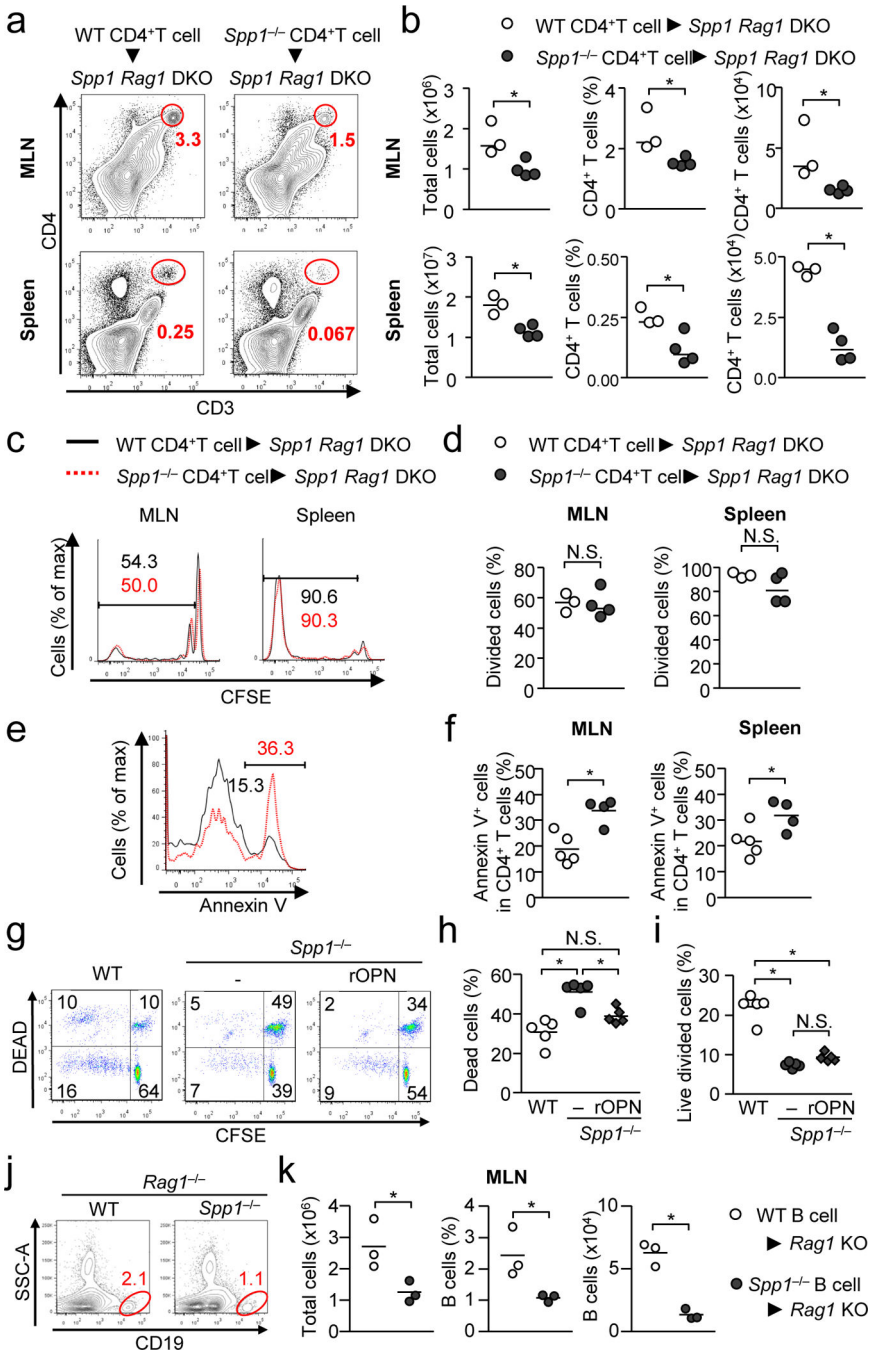

Figure 5. OPN-mediated enhancement of donor lymphocyte survival in lymphopenic recipients

(**a–f**) CD62L^{hi}CD4^{+} T cells (WT or *Spp1*$^{-/-}$) (10^6 per mouse) were transferred to *Spp1*$^{-/-}$*Rag1*$^{-/-}$ mice. Proportion and numbers of CD4^{+} T cells in the MLN and spleen (a, b), proliferation (c, d) and apoptosis of CD4^{+} T cells (e, f) were examined at day 6 (a–d) or day 3 (e, f). Representative flow plots (a, c, e) and analyzed data (b, d, and f) are shown. (**g–i**) Analyzing T cell expansion and death in *ex vivo*. CFSE-labeled CD62L^{hi}CD4^{+} T cells obtained from WT and *Spp1*$^{-/-}$ mice were co-cultured with total MLN cells from *Spp1*$^{-/-}$*Rag1*$^{-/-}$ mice for 7 days in the absence or presence of rOPN (10 ng/ml).

Representative flow images (g), and frequencies of the dead (h) and proliferating $CD4^+$ T cells (i) are shown. (**j, k**) B cells obtained from WT and *Spp1*$^{-/-}$ mice were transferred to *Rag1*$^{-/-}$ mice, and B cells in the MLNs were detected at 4 weeks after transfer. $CD19^+B220^+CD93^-$ mature B cells (2×10^6 per mouse) were used to exclude the contribution of immature B cells, which may develop into mature B cells during experiments Representative flow images (j), and proportions and numbers of B cells in the MLN (k) are shown. All the data is a representative of successfully repeated two independent experiments. * $p<0.05$. Data were analyzed by Student's t-Test (b, d, f, k) and one-way ANOVA (h, i). N.S.; not significant.

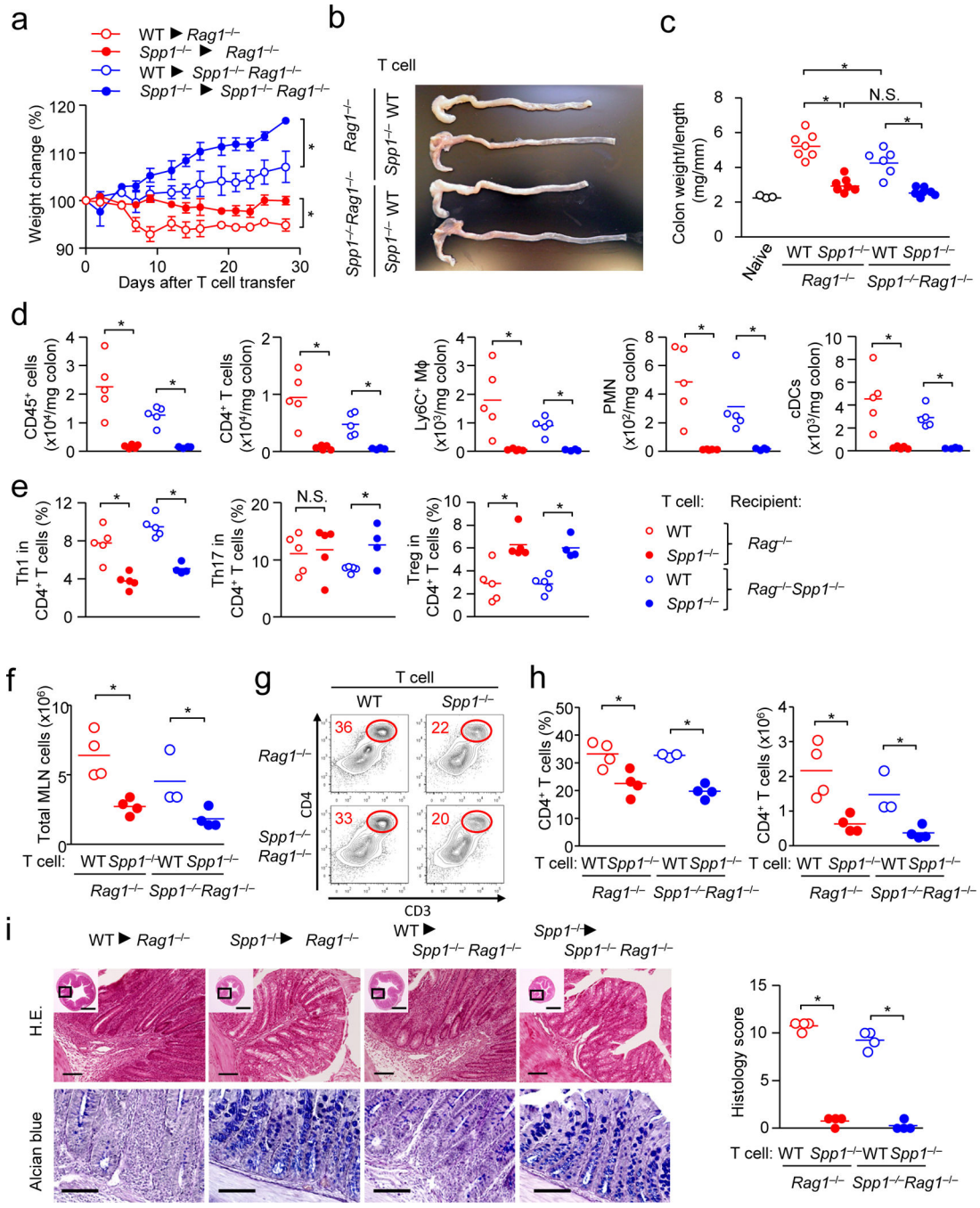

Figure 6. T cell-derived OPN exacerbates T cell-mediated colitis in *Rag1*$^{-/-}$ mice

CD62L^{hi}CD4^{+} T cells (10^6 per mouse) obtained from WT and *Spp1*$^{-/-}$ mice were transferred to *Rag1*$^{-/-}$ or *Spp1*$^{-/-}$*Rag1*$^{-/-}$ recipients. (**a–f**) Weight change (a)(n=3–4 per group), and a representative image of colons (b) are shown. Colitis severity is shown with the colon weight/length ratios (c), and cell infiltration in the colon (d, e) at 4 weeks after T cell transfer. In (d, e), gating was set as CD4^{+} T cells (CD3^{+}CD4^{+}), Ly6C^{+} myeloid cells (CD11b^{+}Ly6C^{+}Ly6G^{-}), neutrophils (CD11b^{+}Ly6G^{+}), cDC (CD11c^{+}B220^{-}), Th1 (CD3^{+}CD4^{+}IFN-γ^{+}), Th17 (CD3^{+}CD4^{+}IL-17^{+}), and Treg (CD3^{+}CD4^{+}Foxp3^{+}). Proportions

of the three T helper subsets are relative to total $CD4^+$ T cells. (**f–h**) Numbers of total MLN cells at 4 weeks after T cell transfer (f), Representative flow panels gated on total leukocytes (g), and frequencies and numbers of $CD4^+$T cells. (i) Histology of colon with histological scores. Scale bars in wide angle and magnified views indicate 1 mm (H&E) or 100 μm (Alcian blue). Datasets in (a–c, f–i) are representatives of successfully repeated three independent experiment. Data in (d, e) was obtained from two independent experiments. Data were analyzed by Student's t-Test (a, d–f, h, i) and one-way ANOVA (c). * $p<0.05$. N.S.; not significant.

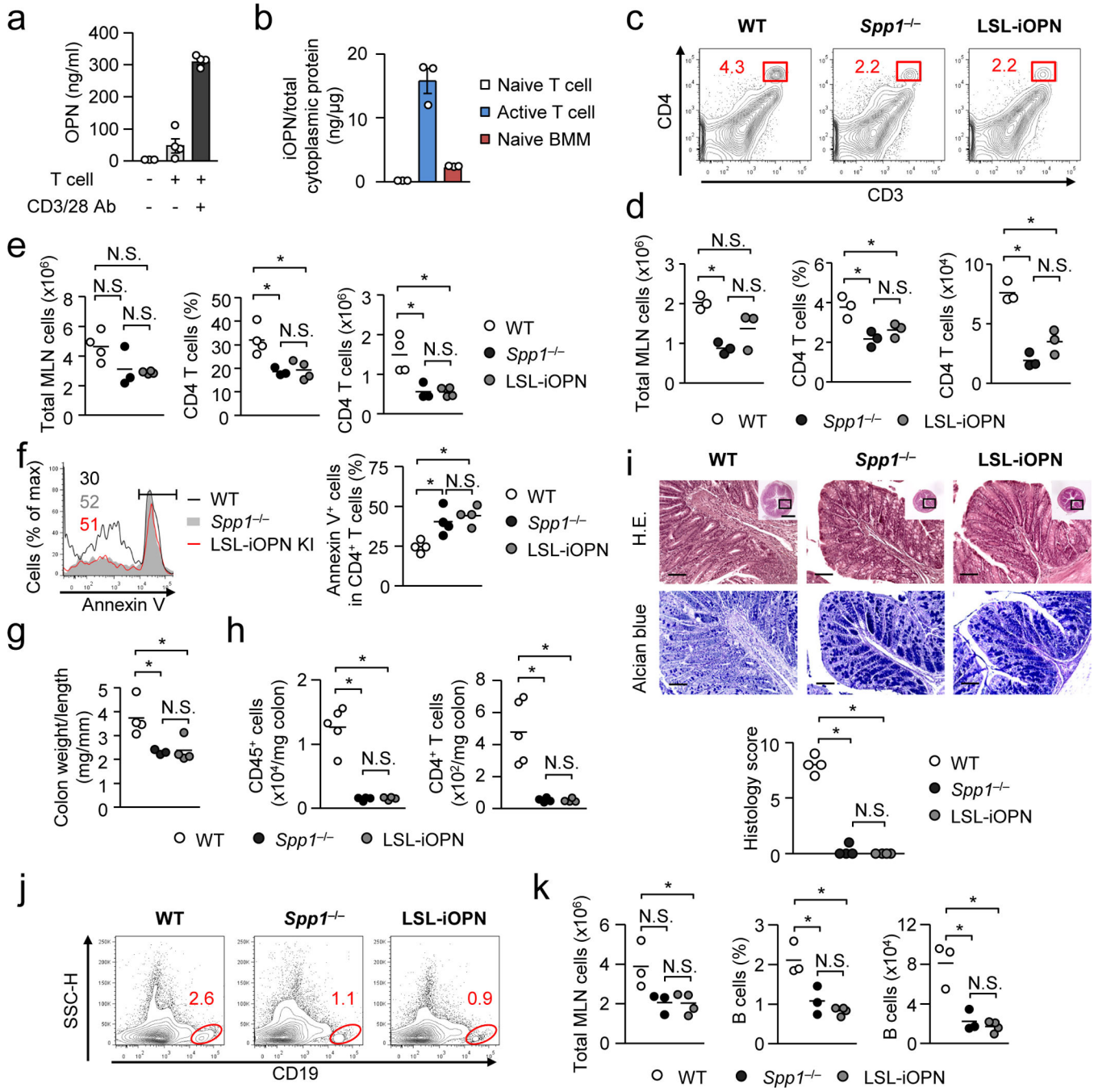

Figure 7. Ruling out iOPN in exacerbating T cell-mediated colitis

(**a**) OPN secretion by T stimulated with anti-CD3/CD28 antibody for 3 days in tissue culture. $CD4^+$ T cells obtained from the MLNs of *Spp1*$^{-/-}$*Rag1*$^{-/-}$ mice 4 weeks after $CD62L^{hi}CD4^+$ T cell transfer. Levels of sOPN were evaluated by ELISA. Error bars denote ± SEM. (**b**) The amount of iOPN per total cytoplasmic proteins in T cells (naive and activated) and BMMs. Cytoplasmic proteins were separated with the Pierce NE-PER reagent. (**c–f**) Colitis was induced by adoptively transferring WT, *Spp1*$^{-/-}$ or LSL-iOPN $CD62L^{hi}CD4^+$ T cells to *Spp1*$^{-/-}$*Rag1*$^{-/-}$ recipients. Total MLN and $CD4^+$ T cells

(CD3$^+$CD4$^+$ of total leukocytes) were enumerated on day 6 (c, d) and day 28 (e). Apoptotic CD4$^+$ T cells in MLNs on day 3 were labeled with Annexin-V (f). (**g–i**) Evaluation of the colon on day 28 after T cell transfer. Colon weight per length (g), CD45$^+$ and CD4$^+$ T cell (CD45$^+$CD3$^+$CD4$^+$) numbers (h), and histology with scores (i) are shown. Scale bars indicate 100 μm (main images) or 1 mm (insets). (**j, k**) Mature B cells (CD19$^+$B220$^+$CD93$^-$) (2×10^6 per mouse) from WT, *Spp1*$^{-/-}$ or LSL-iOPN mice were adoptively transferred to *Rag1*$^{-/-}$ mice. Representative flow plots (j), and the frequencies and numbers of B cells (k) in the MLNs are shown. All datasets are representatives of two independent experiments. N.S.; Not significant. * $p< 0.05$. Data was analyzed by one-way ANOVA (d–i and k).

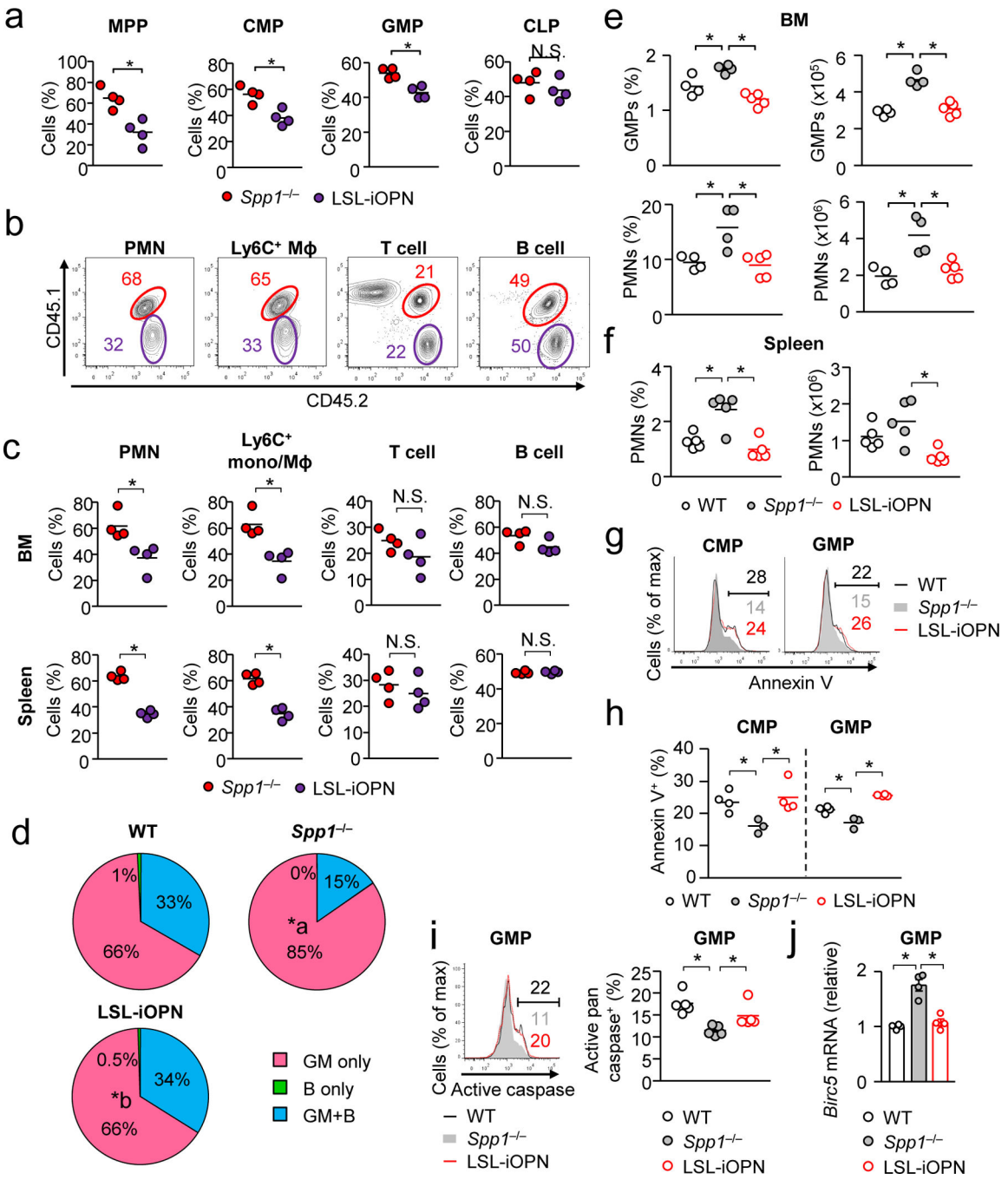

Figure 8. iOPN inhibits myelopoiesis

(**a–c**) Mixed BM chimera mice were generated by transferring BM obtained from *Spp1*$^{-/-}$ (CD45.1/CD45.2) or LSL-iOPN mice (CD45.2) to irradiated WT mice (CD45.1) as shown in Supplementary Fig. 2f, g. The ratio of *Spp1*$^{-/-}$-derived (red) and LSL-iOPN-derived (purple) hematopoietic progenitor (a), myeloid and lymphoid cells (b, c) in the BM were examined at 3 weeks (a) or 7 weeks (b, c) after BM cell transfer. Representative flow images of splenic cells are shown in (b). Data (a, c) is a representative of two independent experiment. Mϕ: macrophage. (**d**) *Ex vivo* single-cell MPP differentiation assay, comparing

WT, *Spp1*$^{-/-}$, and LSL-iOPN MPPs. Development of GM cells between *Spp1*$^{-/-}$ (indicated with “a”) and LSL-iOPN (indicated with “b”) was significantly different ($p < 0.05$) by the Chi-square test. Plating efficiencies were 201 of 506 (40%; WT), 246 of 506 (49%; *Spp1*$^{-/-}$), and 363 of 960 (38%; LSL-iOPN). Data were pooled from two independent experiments. (**e–j**) WT, *Spp1*$^{-/-}$ and LSL-iOPN mice were systemically infected with Candida (2–10^6 spores/mouse). Shown are frequencies and numbers of GMPs (e), neutrophils (f), Annexin-V$^+$ CMPs and GMPs (g, h), pan-caspase activity (i), and *Birc5* expression (j) in GMPs at 15 hrs (g–j) or 24 hrs (e, f) after Candida infection. Each dataset in (e, f, h–j) is a representative of two independent experiments. *; $p < 0.05$. Data was analyzed by the Student’s t-test (a, c) and ANOVA (e, f, h–j). N.S.; not significantly different.